Supporting Information

Pd Supported on Carbon Nitride Boosts the Direct Hydrogen Peroxide Synthesis

Rosa Arrigo,* [†‡] Manfred E. Schuster,[‡] Salvatore Abate,[§] Gianfranco Giorgianni,[§] Gabriele Centi,[§] Siglinda Perathoner,[§] Sabine Wrabetz, [‡] Verena Pfeifer, [‡] Markus Antonietti, [δ] Robert Schlögl, [‡†].

[†] Max-Planck-Institut für Chemische Energiekonversion, Stiftstrasse 34-36, 45470 Mülheim an der Ruhr, Germany

[‡] Fritz-Haber Institut der Max-Planck Gesellschaft, Faradayweg 4-6, 14195 Berlin, Germany

[§] Università degli Studi di Messina, V.le F. Stagno D'Alcontres 31, 98166 Messina, Italy

[δ] Max-Planck-Institut für Kolloid und Grenzflächenforschung, Am Mühlenberg 1 OT Golm, 14476, Potsdam, Germany

*Correspondence to: rosa.arrigo@diamond.ac.uk

Selectivity/CO differential heat of adsorption correlation

Selectivity (S) was correlated to the CO microcalorimetric chemisorption results in order to identify the treshold value of differential heat of chemisorption for the selective path. The following formula was applied and solved analytically:

S= μmol of CO below the treshold value/ μmol of total CO chemisorbed. The $Pd_{1.8\%}$873 after 20 minutes of reaction is characterized by a selectivity of 93%. Thus among the total 2 $\mu mol*g^{-1}$ of CO adsorbing, only 1.86 $\mu mol*g^{-1}$ of CO adsorb on the Pd atoms, which catalyze selectively the O_2 hydrogenation. For the used $Pd_{0.3\%}C_xN$ after 180 minutes of reaction, the selectivity is 58%. In this case, among the 0.16 $\mu mol*g^{-1}$ of CO adsorbing, only 0.96 $\mu mol*g^{-1}$ of CO adsorb on the Pd atoms, which catalyze selectively the O_2 hydrogenation. Those two catalysts actually give a pretty similar threshold value. This corresponds to a threshold value of 70 $kJ*mol^{-1}$: all the sites probed by CO chemisorption above this value are unselective. On the other hand, for $Pd_{1.8\%}$473, if we consider the overall amount of CO adsorbed 3.4 $\mu mol*g^{-1}$, 2.1 $\mu mol*g^{-1}$ are responsible of the unselective pathway which gives a differential heat of adsorption as low as 40 $kJ*mol^{-1}$.

For the sample $Pd_{1.7\%}$473 a better correlation was found when considering only the CO chemisorbed with a heat of adsorption above 40 $kJ*mol^{-1}$. In this case, 1.22 $kJ*mol^{-1}$are considered unselective and 0.78 $kJ*mol^{-1}$ selective. This situation corresponds to a threshold differential heat of chemisorption of about 70 $kJ*mol^{-1}$, consistently with the other samples. If this is the case, chemisorption sites present on the $Pd_{1.7\%}$473 with a differential heat of chemisorption of 40 $kJ*mol^{-1}$ are not involved in the H_2O_2 synthesis from the elements. These chemisorption sites could be intuitively assigned to the Pd^{2+} species highly abundant on this sample. Such a correlation could also explain the initial low activity observed for the PdAuNCNT473 catalysts discussed in reference 6. Those values could be used to model selective and unselective Pd sites and predict better catalysts for the H_2O_2 direct synthesis.

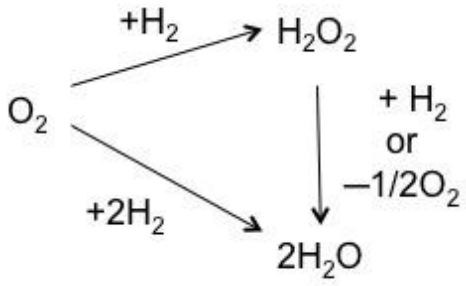

Scheme S 1: Reaction network of the direct H_2O_2 synthesis: direct formation of H_2O_2 and H_2O, and decomposition of H_2O_2 to water.

Table S1. Comparison of the performances in the direct H_2O_2 synthesis as reported in patents[1].

Company	*Catalyst*	*H_2O_2, % wt.*	*Selectivity, %*	*Reaction conditions*
Dupont	Pd-Pt (Pt/Pd+Pt = 0.08) colloidal on alumina	19.6	69	136 bar, 5-8°C, 18% H_2 in O_2, aqueous acid solution (0.1N HCl)
ENI	1% Pd-0.1%Pt on carbon	7.3	74	100 bar, 8°C, (autoclave, after 600h), 3.6% H_2, 11% O_2 in inert 95:5 methanol:H_2O solution (+ additives)
BASF	Pd on monolith	7.0	84	144 bar, 10% H_2 in O_2, methanol (+ additives)
HTI	Pd(-Pt) on carbon black (140 m^2/g)*	9,1 (276 g/g Pd.h)	99	~120 bar, ~35°C, (autoclave, after 600h), 3% H_2 in air solvent and additives not indicated
Degussa	2.5% Pd-Au (95:5) on a-Al2O3	5,1 (13.8 g/g Pd.h)	72	50 bar, 25°C (trickle bed), 3% H_2, 20% O_2 methanol (+ additives)

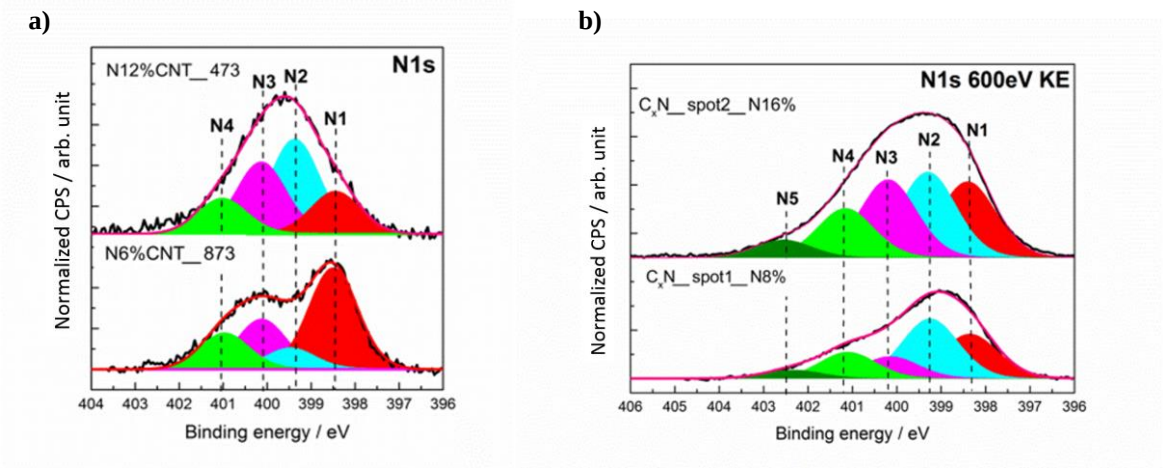

Figure S1. a) Deconvolved N1s XP spectra for NCNT473 (top) and NCNT873 (bottom) at KE 600eV. 12% and 8% are the N atomic abundance for NCNT473 and NCNT873, respectively. Fitting: [11] N1 (398.5 eV) is pyridine-like N; N2 (399.4 eV) is NH bond in amine and amide; N3 (400.1 eV) is pyrrole and lactam species; N4 (401.1 eV) is graphitic N. b) Deconvolved N1s XP spectra for C_xN at KE 600eV in different sample spots. 16% and 8% are the N atomic abundance. The N5 component was attributed to N-O species.

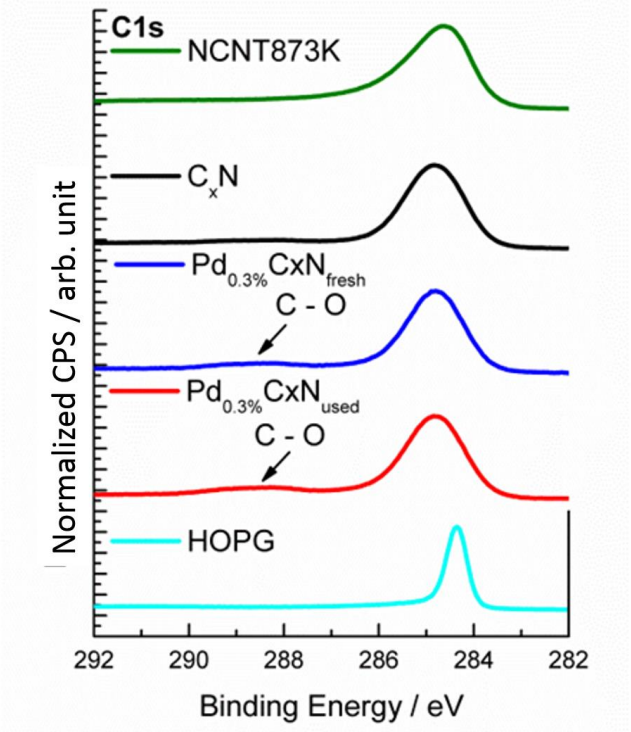

Figure S 2: C1s spectra at 600eV KE, corresponding to a depth information of 2.5nm, normalized at the maximum peak intensity for comparison: C_xN fresh (black line), after Pd immobilization (blue line), $Pd_{0.3\%}C_xN$ used (red line), NCNT functionalized with NH_3 at 873K, NCN873 (green line) and HOPG (pale blue). The C1s spectrum of the NCN873 shows a peak with maximum at 284.5 eV much broader than the asymmetric peak of HOPG at 284.4 eV. Broadening to the higher binding energy side indicates C in sp^3 bonding or highly defective sp^2 carbon phase. C-N species contribute to this broadening. The C_xN samples are characterized by a more symmetric main peak than the NCNT873, with maximum at 285 eV, indicating a comparatively reduced extension of the conjugated π–system. The component around 288 eV is attributed to parasitic surface C-O species. [11]

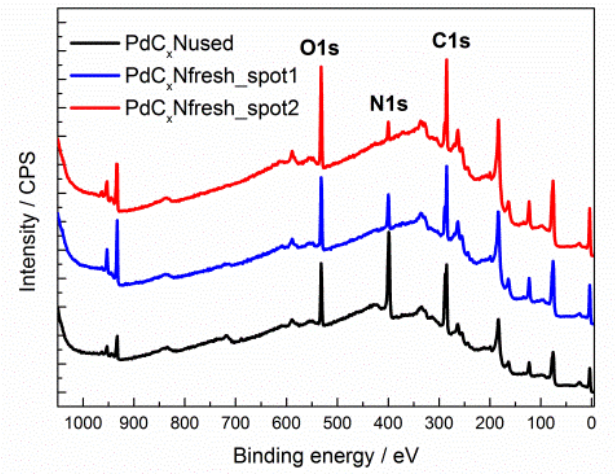

Figure S 3: Survey spectra with 1100 eV excitation energy for $Pd_{0.3\%}C_xN$ fresh (red and blue line) and $Pd_{0.3\%}C_xN$ used (black).

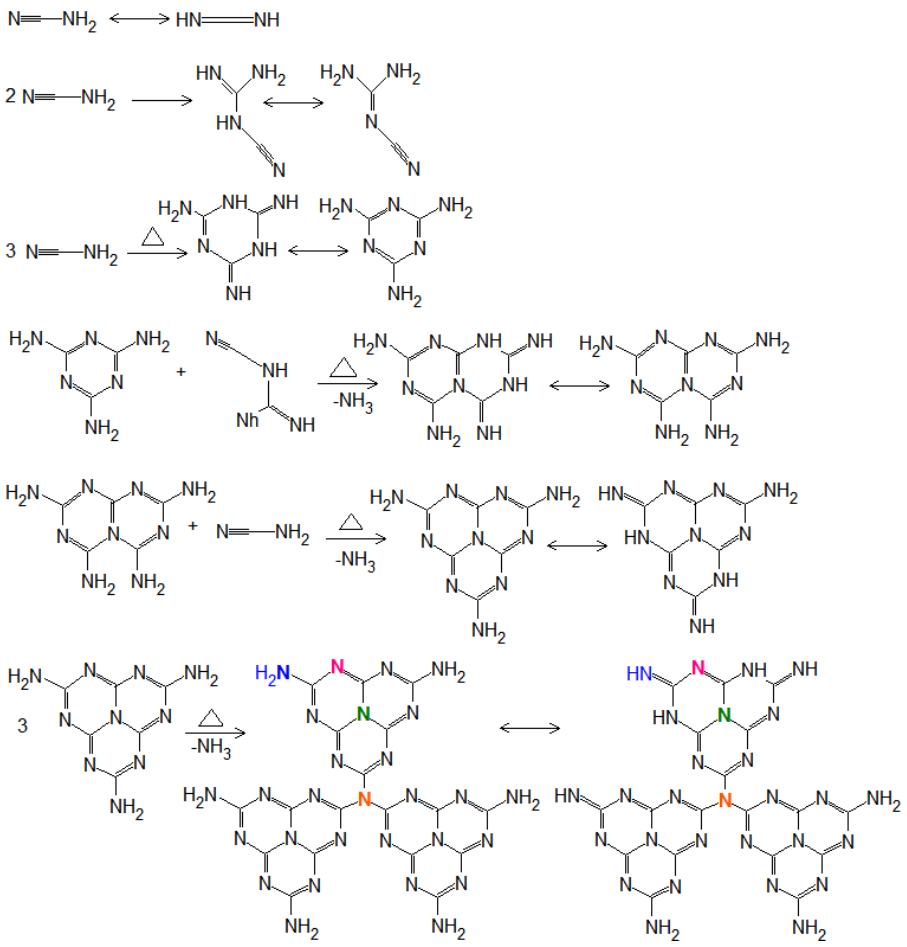

Scheme S 2: Proposed formation pathways of the different N species in C_xN.

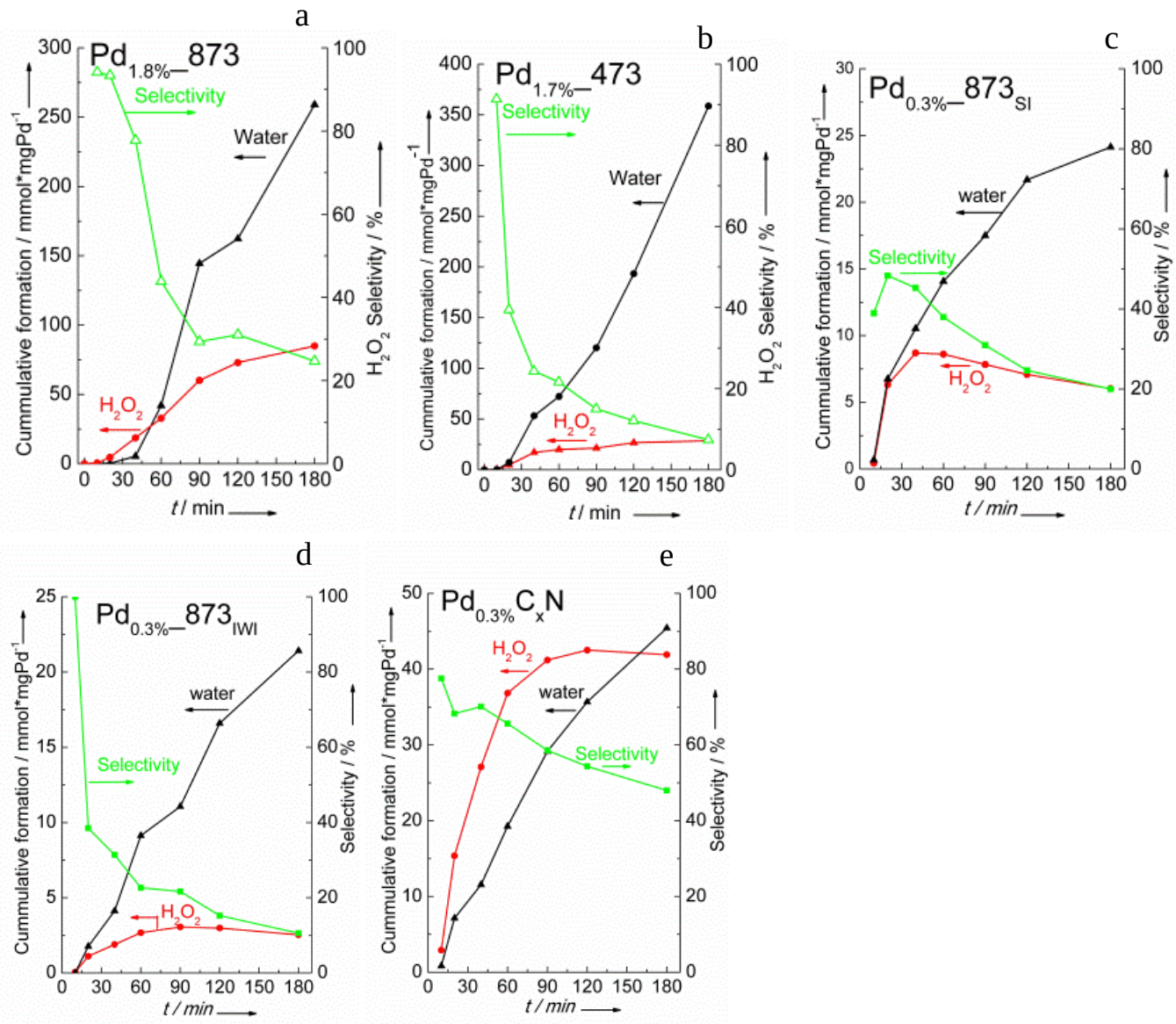

Figure S 4: Cumulative formation of H_2O_2 (red cycle), cumulative formation of H_2O (black cycle) and H_2O_2 selectivity (green cycle) for $Pd_{1.8\%}873$ (a); $Pd_{1.8\%}473$ (b); $Pd_{0.3\%}873_{SI}$ (c) $Pd_{0.3\%}873_{IWI}$ (d) and $Pd_{0.3\%}C_xN$ (e). Changes in selectivity are triggered by the excessive exposure of the Pd surface to the reactive environment, O_2 and H_2, which is realized by the initial detachment of the PVA covering the nanoparticles surface facilitating the NPs overgrowth. This is the dominant process for most of the Pd NPs on NCNTs, due to the very low abundance of substitutional N species stabilizing small nanoparticles and, the more rigid carbon structure of the support. On C_xN, the higher N abundance and the poorly graphitic surface realize a condition in which the surface of the Pd NPs is protected even at long reaction time resulting in the higher selectivity observed.

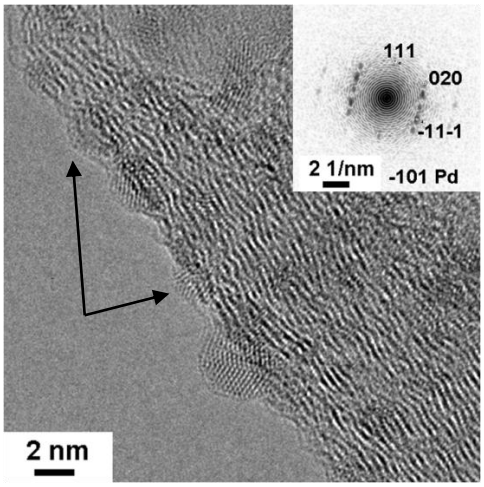

Figure S 5. HRTEM image and FFT (inset) of fresh $Pd_{1.8\%}873$. The arrows indicate nanoparticles with rough-like morphology.

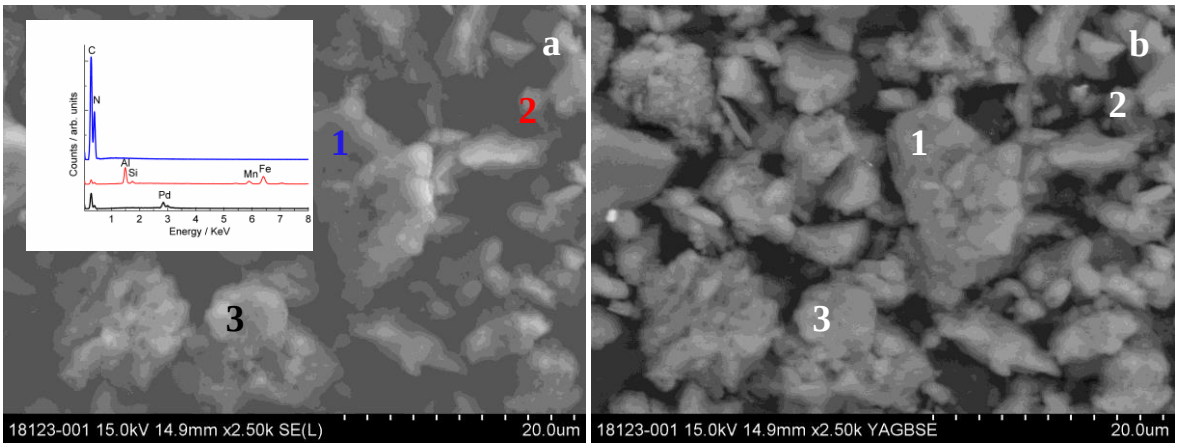

Figure S 6: SE (a) and BSE (b) images for $Pd_{0.3\%}C_xN$ fresh at 15 kV. Local EDX spectra corresponding to point 1 (blue spectrum), point 2 (red spectrum) and point 3 (black spectrum) are reported in the inset of Figure S6a. It is interesting to note that Pd is not detected where impurities of Al and Fe are present.

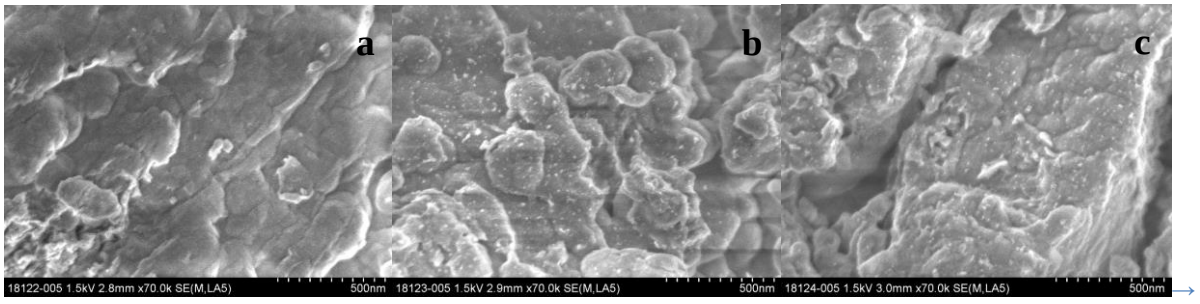

Figure S 7: Scanning electron micrograph at 1.5 kV of C_xN (a); $Pd_{0.3\%}C_xN$ fresh (b) and $Pd_{0.3\%}C_xN$ used after 180 minutes of reaction (c).

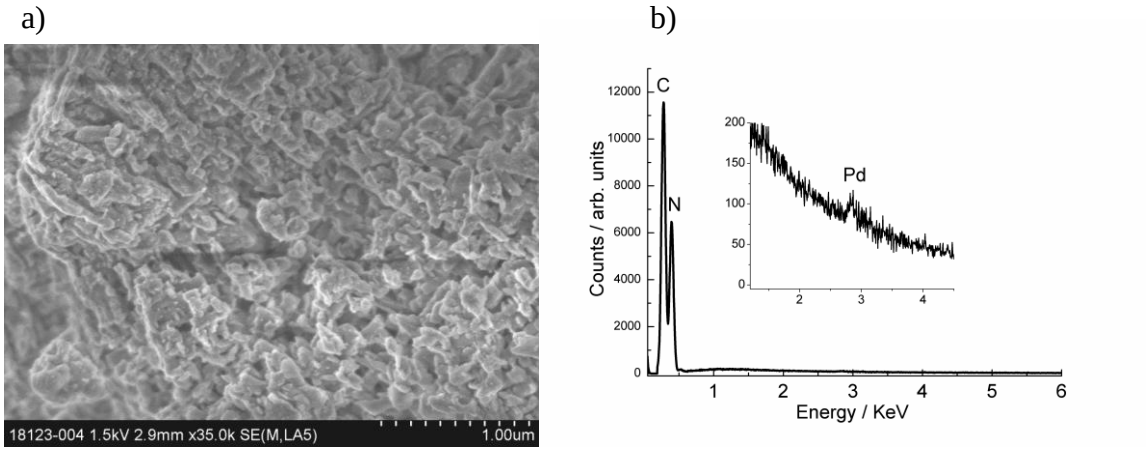

Figure S 8: SE image of $Pd_{0.3\%}C_xN$ at 1.5 kV (a) and corresponding EDX spectrum (b). The EDX spectrum quantification in weight percentage is: 69% C, 29.4% N, 1% O, 0.4% Pd.

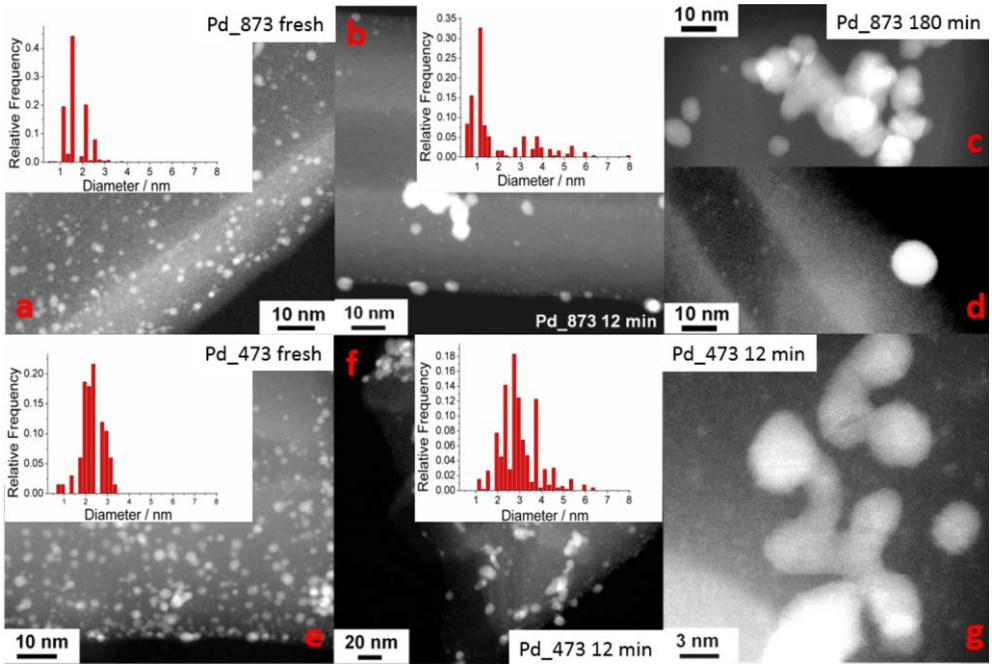

Figure S 9 HAADF-STEM image and derived particle size distribution (insets) of Pd/NCNT: fresh $Pd_{1.8\%}873$ (a); 12 min (b) 180 minutes (c, d); fresh $Pd_{1.7\%}473$ (e); 12 minutes (f, g).

.

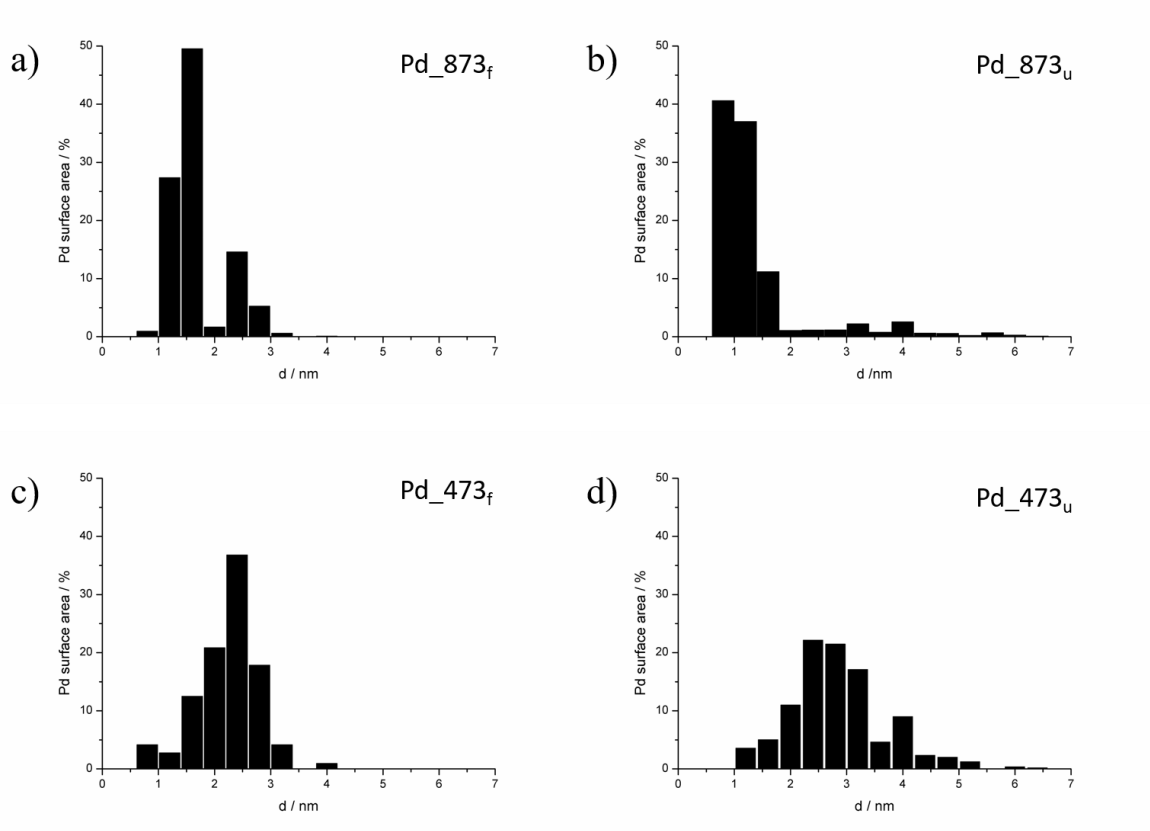

Figure S 10. Fractional distribution of surface area of Pd particles derived from the particle size distribution obtained in STEM images (Insets Figure S9)

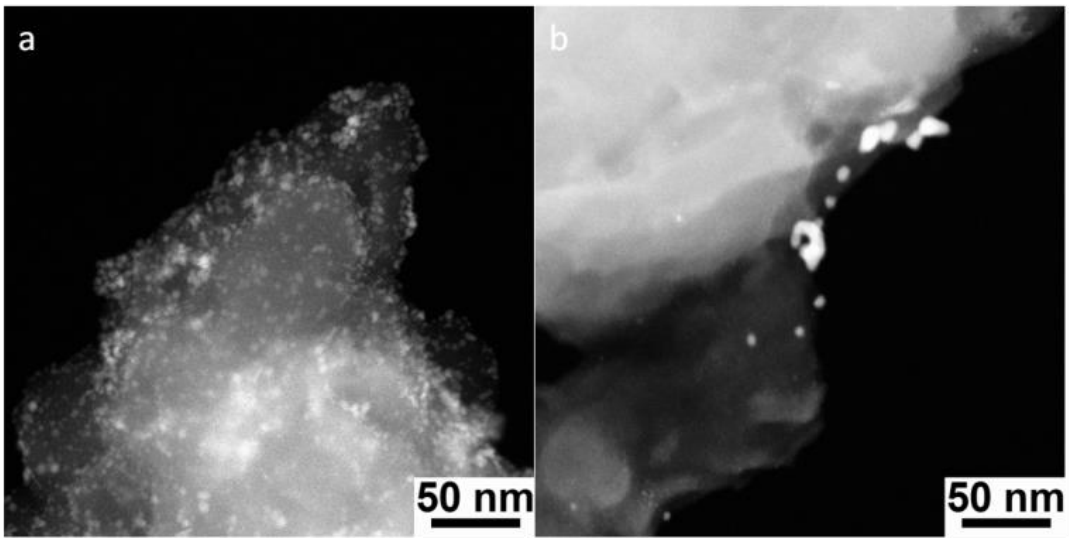

Figure S 11: HAADF-STEM image fresh $Pd_{0.3\%}C_xN$ (a) and used after 180 minutes of reaction (b**).**

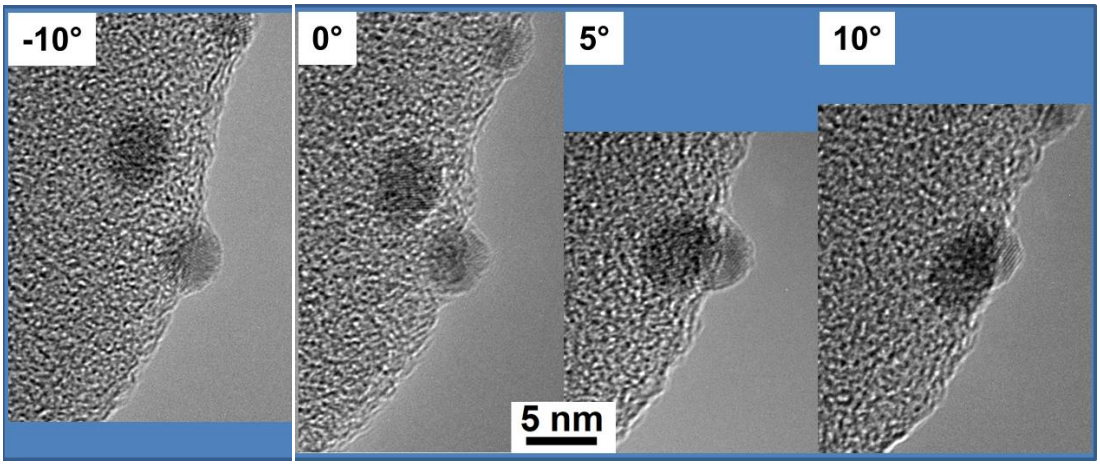

Figure S 12: Tilting series of HRTEM images for a NP of the $Pd_{0.3\%}C_xN_{used}$. Note the omnipresence of the carbonaceous fragments at both sides of the NPs.

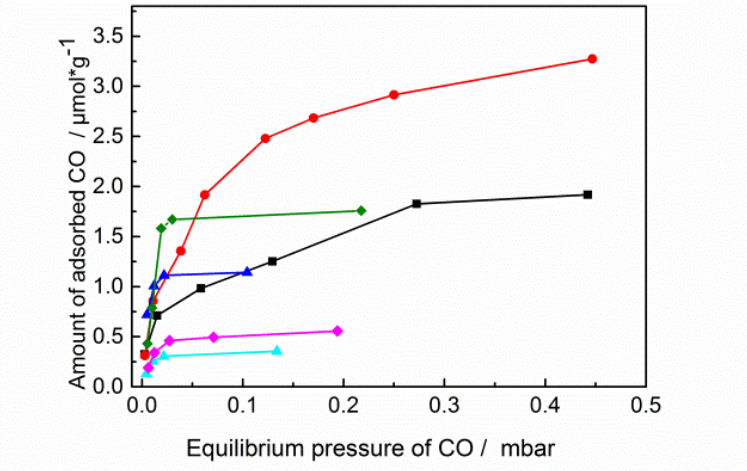

Figure S 13: Adsorption isotherm for: $Pd_{1.8\%}873$ used after 12 minutes of reaction (black square); $Pd_{1.7\%}473$ used after 12 minutes of reaction (red circle); $Pd_{0.3\%}873_{IWI}$ fresh (magenta rhombus); $Pd_{0.3\%}C_xN$ fresh (pale blue triangle); 1st cycle of CO adsorption on $Pd_{0.3\%}C_xN$ used after 180 minutes of reaction (green rhombus) and 2nd cycle of CO adsorption after desorption step (blue triangle). The best fit of the isotherms is the Langmuir isotherm model.

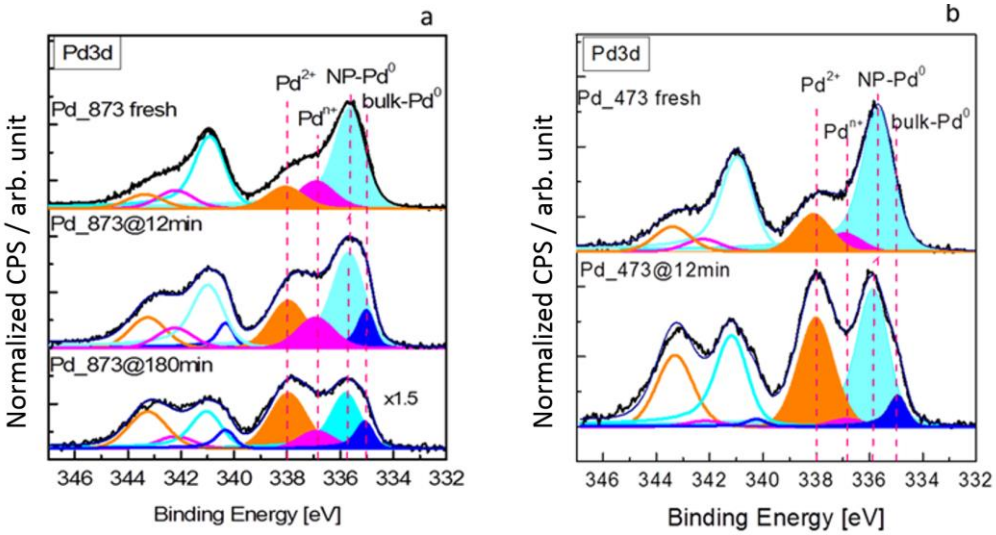

Figure S 14. XP Pd3d spectra of $Pd_{1.8\%}873$ (left panel) and $Pd_{1.7\%}473$ (right panel) as fresh and used catalyst. Fitting: [6, 13] bulk-like Pd^0 (335.1 eV); NP Pd^0 (335.55 eV); Pd^{n+} at NP Pd^0 surface (336.9 eV); ionic Pd^{2+} (338 eV).

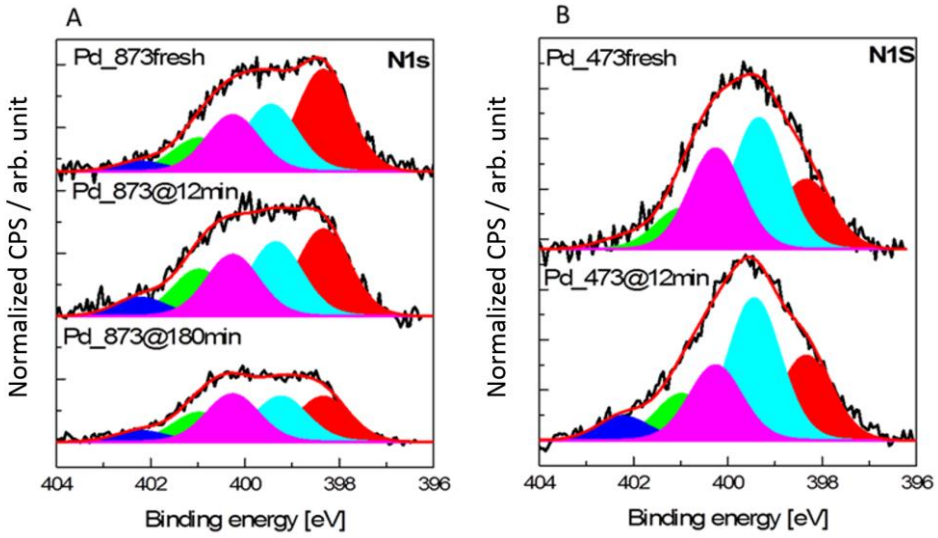

Figure S 15: N1s XP spectra for fresh (bottom) and after 12min reaction (top): $Pd_{1.8\%}873$ (A) and $Pd_{1.7\%}473$(B). Fitting as described in [11, 13]: N1 (red) Pyridine-like N; N2 (blue light) NH in amine and amide; N3 (magenta) in pyrrole-like and lactam N; N3 (green) quaternary N; N5 (dark blue) Pyridine oxide species.

Table S2. N and Pd total absolute abundance and relative abundance of Pd species from XPS

Catalyst	N (at%)	Pd (at%)	Pd components (%)			
			bulk-like Pd^0 (335.1 eV)	NP Pd^0 (335.55 eV)	PdO_x at Pd^0 surface (336.9 eV)	ionic Pd^{2+} (338 eV)
$Pd_{1.7\%}473$_fresh	4.7	1.5	0	79	7	14
$Pd_{1.8\%}873$_fresh	3.1	1.9	0	76	13	11
$Pd_{1.7\%}473$_12min	4.6	1.5	18	33	3	46
$Pd_{1.8\%}873$_12min	3.5	1.6	9	58	14	19
$Pd_{1.8\%}873$_180min	3.9	0.76	15	43	10	32